J|A|C|S
ARTICLES

Published on Web 06/03/2008

Quantifying Two-Bond $^1HN-^{13}CO$ and One-Bond $^1H^{\alpha}-^{13}C^{\alpha}$ Dipolar Couplings of Invisible Protein States by Spin-State Selective Relaxation Dispersion NMR Spectroscopy

D. Flemming Hansen, Pramodh Vallurupalli, and Lewis E. Kay*

Departments of Molecular Genetics, Biochemisty, and Chemistry, University of Toronto, Toronto, Ontario, Canada, M5S 1A8

Received February 8, 2008; E-mail: kay@pound.med.utoronto.ca

Abstract: Relaxation dispersion NMR spectroscopy has become a valuable probe of millisecond dynamic processes in biomolecules that exchange between a ground (observable) state and one or more excited (invisible) conformers, in part because chemical shifts of the excited state(s) can be obtained that provide insight into the conformations that are sampled. Here we present a pair of experiments that provide additional structural information in the form of residual dipolar couplings of the excited state. The new experiments record ^1H spin-state selective ^{13}CO and $^{13}C^{\alpha}$ dispersion profiles under conditions of partial alignment in a magnetic field from which two-bond $^1HN-^{13}CO$ and one-bond $^1H^{\alpha}-^{13}C^{\alpha}$ residual dipolar couplings of the invisible conformer can be extracted. These new dipolar couplings complement orientational restraints that are provided through measurement of $^1HN-^{15}N$ residual dipolar couplings and changes in ^{13}CO chemical shifts upon alignment that have been measured previously for the excited-state since the interactions probed here are not collinear with those previously investigated. An application to a protein−ligand binding reaction is presented, and the accuracies of the extracted excited-state dipolar couplings are established. A combination of residual dipolar couplings and chemical shifts as measured by relaxation dispersion will facilitate a quantitative description of excited protein states.

Introduction

In the past decade there have been a number of very significant methodological developments that have impacted solution nuclear magnetic resonance (NMR) studies of biomolecules. First, methods have been introduced for weak alignment of molecules,[1–5] along with experiments that measure the resultant residual anisotropic magnetic interactions with high sensitivity.[6–8] Such interactions can be quantified to produce restraints that define the orientation of dipolar interaction vectors[1,9] or chemical shift tensors[10] with respect to a molecule-based frame. Because all measurables relate to the same molecular frame,[1,9] they can provide long-range information that connects elements of structure that are separated by many angstroms, unlike many other types of restraints typically measured in NMR studies that are sort-range in nature, such as nuclear Overhauser effects and scalar couplings.[11] A second major contribution has been the development of 2D and 3D correlation experiments that transfer magnetization between coupled spins or record chemical shifts in a spin-state selective manner.[12] Often it is possible to achieve appreciable gains in both spectral sensitivity and in resolution by choosing the appropriate spin-state. This so-called TROSY effect was originally developed for applications involving amide $^1HN-^{15}N$ spin pairs[13] but subsequently extended to more complex spin-systems such as $^{13}CH_3$ (ref 14) and $^{13}CH_2$ (ref 15) groups.

The two contributions highlighted above can be combined to advantage. For example, in the past several years, a variety of spin-state selective experiments have been developed for the measurement of residual anisotropic interactions.[16–18] More recently, it has been shown that it is possible to combine spin-state selection and molecular alignment with experiments that

(1) Tjandra, N.; Bax, A. *Science* **1997**, *278*, 1111–1114.
(2) Hansen, M. R.; Mueller, L.; Pardi, A. *Nat. Struct. Biol.* **1998**, *5*, 1065–1074.
(3) Clore, G. M.; Starich, M. R.; Gronenborn, A. M. *J. Am. Chem. Soc.* **1998**, *120*, 10571–10572.
(4) Sass, H. J.; Musco, G.; Stahl, S. J.; Wingfield, P. T.; Grzesiek, S. *J. Biomol. NMR* **2000**, *18*, 303–309.
(5) Tycko, R.; Blanco, F. J.; Ishii, Y. *J. Am. Chem. Soc.* **2000**, *122*, 9340–9341.
(6) Prestegard, J. H.; Mayer, K. L.; Valafar, H.; Benison, G. C. *Methods Enzymol.* **2005**, *394*, 175–209.
(7) Bax, A.; Kontaxis, G.; Tjandra, N. *Methods Enzymol.* **2001**, *339*, 127–174.
(8) Bax, A. *Protein Sci.* **2003**, *12*, 1–16.
(9) Tolman, J. R.; Flanagan, J. M.; Kennedy, M. A.; Prestegard, J. H. *Proc. Natl. Acad. Sci. U.S.A.* **1995**, *92*, 9279–9283.
(10) Cornilescu, G.; Marquardt, J.; Ottiger, M.; Bax, A. *J. Am. Chem. Soc.* **1998**, *120*, 6836–6837.
(11) Wüthrich, K. *NMR of Proteins and Nucleic Acids*; John Wiley & Sons: New York, 1986.
(12) Wider, G.; Wüthrich, K. *Curr. Opin. Struct. Biol.* **1999**, *9*, 594–601.
(13) Pervushin, K.; Riek, R.; Wider, G.; Wüthrich, K. *Proc. Natl. Acad. Sci. U.S.A.* **1997**, *94*, 12366–12371.
(14) Tugarinov, V.; Hwang, P.; Ollerenshaw, J.; Kay, L. E. *J. Am. Chem. Soc.* **2003**, *125*, 10420–10428.
(15) Miclet, E.; Williams Jr, D. C.; Clore, G. M.; Bryce, D. L.; Boisbouvier, J.; Bax, A. *J. Am. Chem. Soc.* **2004**, *126*, 10560–10570.
(16) Yang, D.; Venters, R. A.; Mueller, G. A.; Choy, W. Y.; Kay, L. E. *J. Biomol. NMR* **1999**, *14*, 333–343.
(17) Kontaxis, G.; Clore, G. M.; Bax, A. *J. Magn. Reson.* **2000**, *143*, 184–196.
(18) Permi, P.; Rosevear, P. R.; Annila, A. *J. Biomol. NMR* **2000**, *17*, 43–54.

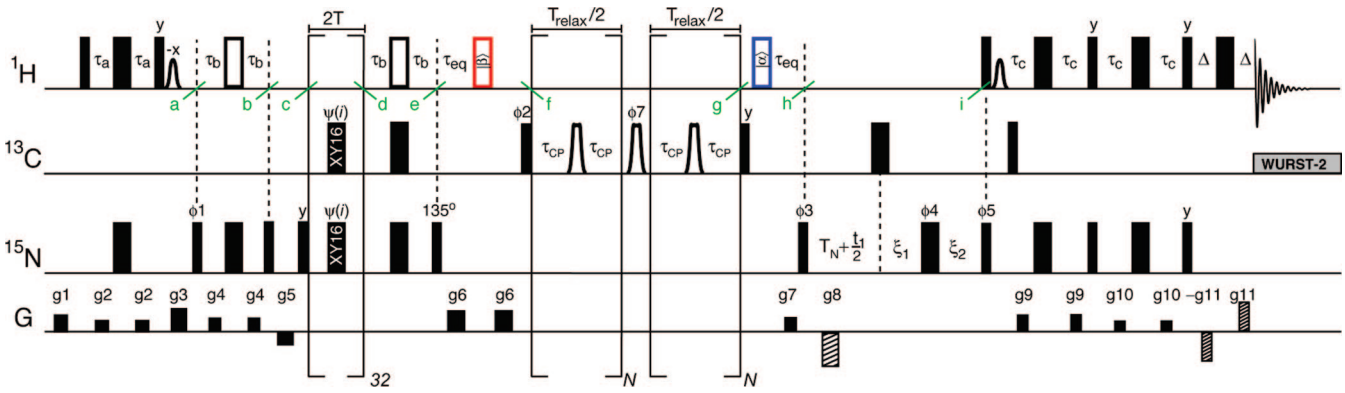

Figure 1. Spin-state selective pulse scheme for the measurement of carbonyl relaxation dispersion profiles derived from magnetization of the form $4C_OT_NZ_NHN^{|\beta\rangle}$ or $4C_OT_NZ_NHN^{|\alpha\rangle}$. ^{1}H, ^{13}C, and ^{15}N 90° (180°) rf pulses are shown as narrow (wide) black bars and are centered on water (^{1}H), 175 ppm (^{13}C), and 119 ppm (^{15}N); the open rectangles indicate composite 180° pulses[44] ($90_x-180_y-90_x$). The transverse relaxation of $4C_OT_NZ_NHN^{|\beta\rangle}$ is measured by applying the (red) composite 180° proton pulse just after point *e* (but not the blue pulse at *g*) whereas relaxation rates of $4C_OT_NZ_NHN^{|\alpha\rangle}$ are obtained using a sequence containing the (blue) composite 180° proton pulse at *g* (but not the red pulse). ^{1}H and ^{15}N pulses are applied at the highest possible power level, whereas all ^{13}C pulses (both those that are rectangular and the shaped RE-BURP[45] pulses during the CPMG element between *f* and *g*) use a 16 kHz field. The use of ^{13}CO-selective RE-BURP pulses during the CPMG element refocuses small (2 or more bond) ^{13}CO-aliphatic carbon couplings that arise from the labeling scheme employed. The shaped 90° ^{1}H pulse of phase $-x$ just prior to *a* and the shaped 90° ^{1}H pulse immediately after *i* are water-selective pulses (~1.5 ms rectangular pulses). Each of the simultaneous 32 pulses labeled XY16 has phase $\Psi(i)=2\{x, y, x, y, y, x, y, x, -x-y,-x,-y,-y,-x,-y,-x\}$ (i.e., pulse 1 is phase *x*, pulse 2 is phase *y*, pulse 3 is phase *x*, etc.) so that both the *x* and the *y* components of the transverse magnetization are refocused properly in the presence of off-resonance effects and pulse imperfections.[46] A WURST-2 ^{13}CO decoupling scheme is employed during acquisition to suppress ^{1}HN$-^{13}$CO scalar/dipolar couplings[47] (bandwidth of 12 ppm, centered at 175 ppm, maximum (rms) B_1 field of 0.5(0.3) kHz). The phase cycle is (Varian), $\phi1=\{45°,225°\}$; $\phi2 = 2\{y\},2\{-y\}$; $\phi3 = \{y\}$; $\phi4 = 4\{x\},4\{-x\}$; $\phi5 = \{x\}$, $\phi7 = \{y,-y\}$, receiver $= \{x,-x,-x,x\}$. The delays used are, $\tau_a = 2.25$ ms, $\tau_b = 1/(8|J_{NH}|) \approx 1.34$ ms, $\tau_c = 1/(4|J_{NH}|) \approx 2.68$ ms, $\tau_{eq} = 5$ ms (the τ_{eq} delay ensures that magnetization reports on equilibrium values at the start/end of the CPMG period), $T = 12$ ms, $T_N = 14$ ms, $\xi_1 = \max(0, t_1/2 - T_N)$, $\xi_2 = \max(0, T_N - t_1/2)$, and $\Delta = 0.5$ ms. *N* can be any whole number. Artifacts due to off-resonance effects of pulses during the CPMG train are suppressed by the pulse of phase $\phi7$.[48] Gradient strengths G/cm (length in ms) are: $g1 = 8.0(0.5)$; $g2 = 4.0(0.5)$; $g3 = 10.0(1.0)$; $g4 = 7.0(0.3)$; $g5 = -6.0(0.6)$; $g6 = 12.0(1.0)$; $g7 = 4.0(0.3)$; $g8 = -30.0(1.25)$; $g9 = 5.0(0.3)$; $g10 = 3.0(0.2)$; $g11 = 28.65(0.065)$. Quadrature detection in the indirect ^{15}N dimension is obtained by recording two set of spectra with ($\phi5$,*g*8) and ($\phi5 + \pi$; $-g8$) for each t_1 increment[49,50] the phase $\phi3$ is incremented along with the receiver phase by π for each complex t_1 point in a TPPI manner.[51]

probe conformational exchange between different states in proteins[19] or in small molecules,[20] providing structural information about excited states that are often recalcitrant to study by other techniques. In these so-called spin-state selective Carr−Purcell−Meiboom−Gill[21,22] (CPMG) relaxation dispersion experiments recorded under conditions of weak molecular alignment, the effective relaxation rates of nuclear probes, $R_{2,\text{eff}}$, are monitored as a function of the rate of application of refocusing pulses (ν_{CPMG}) during an interval of fixed duration. In cases where exchange is between a predominant conformation (ground state) and a low populated (excited) state on a millisecond time-scale, and where the population of the excited-state exceeds 0.5%, the relaxation rate is a sensitive function of the pulse separation.[23] Under these conditions, it becomes possible to extract *both* chemical shift and dipolar coupling differences between states from which chemical shifts and dipolar couplings in the excited-state are obtained,[19,20] despite the fact that this state is frequently not observable. Our group has shown that accurate ^{1}HN$-^{15}$N dipolar couplings could be measured in a pair of applications involving (i) protein folding and (ii) ligand binding using spin-state selective ^{15}N CPMG relaxation dispersion spectroscopy.[19] Subsequently, we have also shown that changes in carbonyl (^{13}CO) chemical shifts of the excited-state upon alignment can be measured that provide quantitative information about the relative orientation of the molecular alignment and chemical shift frames.[24] Since the orientation of the ^{13}CO chemical shift tensor in the peptide frame has been quantified through solution[25] and solid state[26] NMR experiments, changes in ^{13}CO shifts upon alignment provide additional structural restraints.

Our goal here is to supplement existing ^{15}N residual dipolar coupling (RDC) and ^{13}CO residual chemical shift anisotropy (RCSA) experiments that probe the structure of the invisible, excited-state with additional methods that quantify interactions that are noncollinear with those previously proposed. To this end we present CPMG relaxation dispersion experiments for measuring one-bond ^{1}H$^\alpha-^{13}$C$^\alpha$ and two-bond ^{1}HN$-^{13}$CO RDCs in protein samples that are selectively ^{13}C$^\alpha$ or ^{13}CO labeled, respectively. The methodology is applied to the study of a protein−ligand exchanging system and the accuracy of the presented experiments established. The combination of ^{1}H$-^{15}$N, ^{1}H$^\alpha-^{13}$C$^\alpha$, ^{1}HN$-^{13}$CO RDCs, and ^{13}CO RCSAs and backbone ^{1}HN, ^{15}N, ^{13}C$^\alpha$, and ^{13}CO chemical shifts of the excited-state opens up the possibility for a description of its structure at a level previously not possible.

Materials and Methods

Protein Sample Preparation. The Abp1p SH3 domain[27−29] (58 residues) and a 17-residue fragment (KKTKPTPPPKPSHLKPK)

(19) Vallurupalli, P.; Hansen, D. F.; Stollar, E. J.; Meirovitch, E.; Kay, L. E. *Proc. Natl. Acad. Sci. U.S.A.* **2007**, *104*, 18473–18477.
(20) Igumenova, T. I.; Brath, U.; Akke, M.; Palmer, A. G. *J. Am. Chem. Soc.* **2007**, *129*, 13396–13397.
(21) Carr, H. Y.; Purcell, E. M. *Phys. Rev.* **1954**, *4*, 630–638.
(22) Meiboom, S.; Gill, D. *Rev. Sci. Instrum.* **1958**, *29*, 688–691.
(23) Palmer, A. G.; Kroenke, C. D.; Loria, J. P. *Methods Enzymol.* **2001**, *339*, 204–238.
(24) Vallurupalli, P.; Hansen, D. F.; Kay, L. E. *J. Am. Chem. Soc.* **2008**, *130*, 2734–2735.
(25) Cornilescu, G.; Bax, A. *J. Am. Chem. Soc.* **2000**, *122*, 10143–10154.
(26) Teng, Q.; Iqbal, M.; Cross, T. A. *J. Am. Chem. Soc.* **1992**, *114*, 5312–5321.
(27) Rath, A.; Davidson, A. R. *Protein Sci.* **2000**, *9*, 2457–2469.
(28) Lila, T.; Drubin, D. G. *Mol. Biol. Cell* **1997**, *8*, 367–385.
(29) Drubin, D. G.; Mulholland, J.; Zhu, Z. M.; Botstein, D. *Nature* **1990**, *343*, 288–290.

from the yeast protein Ark1p[30] were expressed separately in *Escherichia coli* BL21(DE3) cells, as described previously.[19] Labeling of the Abp1p SH3 domain was achieved by growing cells in M9 minimal media supplemented with $^{15}NH_4Cl$ as the sole nitrogen source and the appropriate carbon source, depending on the sample. Production of a ^2H, ^{15}N, ^{13}CO enriched sample was achieved using [1-^{13}C]-pyruvate and $NaH^{13}CO_3$ as the carbon sources, with growth in 99.9% ^2H_2O, as described in detail in a previous publication.[31] Samples prepared in this manner have isolated ^{13}CO spins with the exception of Leu and His that are not labeled at the carbonyl position. A second sample that is ^{15}N, $^{13}C^\alpha$ labeled (fully protonated) was prepared using [2-^{13}C]-glucose as the sole carbon source,[32] and protein was expressed in ^1H_2O media. As described previously,[32] this approach generates isolated $^{13}C^\alpha$ labeling at all residues with the exception of Ile, Leu, and Val, where C^β is partially isotopically enriched.

Four NMR samples were prepared, two with the $^{13}C^\alpha$ labeling and two with ^{13}CO labeling. All samples contained 50 mM sodium phosphate pH 7.0, 100 mM NaCl, 1 mM EDTA, 1 mM NaN_3, 90%H_2O/10%D_2O (^{13}CO) or 100% D_2O ($^{13}C^\alpha$), with protein concentrations of ~1.4 mM. Two $^{13}C^\alpha$ (^{13}CO) samples were prepared by adding approximately 7% mole fraction Ark1p peptide (for relaxation dispersion CPMG measurements of RDCs of the invisible bound state) or ~100% Ark1p peptide (for direct measurements of RDCs of the highly populated bound state). Mole fractions of bound peptide were initially estimated from the K_D of the SH3 domain-peptide interaction ($K_D = 0.55 \pm 0.05$ μM) that was obtained from isothermal calorimetry and the known peptide/protein concentrations that were based on absorbance measurements. The fraction of bound peptide was subsequently quantified more rigorously from relaxation dispersion measurements. After measurements were recorded in isotropic solution, alignment was achieved by adding Pf1 phage (ASLA biotech) to each of the four samples and the degree of residual alignment initially estimated from the deuterium splitting: 15(18) Hz for the 7% (100%) bound $^{13}C^\alpha$ sample; 55(38) Hz for the 7%(100%) bound ^{13}CO sample.

Data Acquisition. Carbonyl carbon relaxation dispersion profiles were recorded (25 °C) on the selectively ^{13}CO labeled sample described above using spin-state selective pulse schemes (see below) that measure the relaxation of coherences of the form $4CO_XN_ZHN|\beta\rangle$ and $4CO_XN_ZHN|\alpha\rangle$ ($4A_XB_ZC|\kappa\rangle$ denotes single-quantum 3-spin coherence, where $A = ^{13}CO$, $B = ^{15}N$, and $C = ^1HN|\kappa\rangle$ refer to the ^{13}CO spin of residue j, the ^{15}N and ^1HN spins of residue $j+1$ and $\kappa \in \{\alpha,\beta\}$ indicates the spin-state of ^1HN). An additional ^{13}CO dispersion experiment was performed that was not ^1HN spin-state selective (coherences of the form $2CO_XN_Z$), using a scheme that has been described in detail previously.[31] Dispersion profiles comprising fifteen values (two duplicate points) of ν_{CPMG} between 33 and 1000 Hz (see below), $T_{relax} = 30$ ms, were recorded on Varian Inova 11.7 T (500 MHz) and 18.8 T (800 MHz) spectrometers equipped with room temperature probe-heads. Each of the data sets for measuring the spin-state selective dispersion profiles ($4CO_XN_ZHN|\beta\rangle$ and $4CO_XN_ZHN|\alpha\rangle$) was recorded in 30(26) hours at 11.7 T(18.8 T), whereas the "$2CO_XN_Z$ data set" was recorded in 39(16) hours at 11.7(18.8)T.

$^1NH-^{13}CO$ two-bond RDCs were recorded directly on the fully bound protein sample from a pair of TROSY-based HNCO data sets[33] (only ^{13}CO, ^1HN planes were acquired) where carbonyl magnetization of the form $4CO_XN_ZHN|\beta\rangle$ or $4CO_XN_ZHN|\alpha\rangle$ was prepared and allowed to evolve during t_1. The displacement of correlations in the ^{13}CO dimension provides a direct measure of $J_{CO,NH} + D_{CO,NH}$. Values of $J_{CO,NH}$ were not measured but were assumed to be 4.4 Hz, based on previous studies by our laboratory showing that $J_{CO,NH}$ is relatively uniform in proteins[16] (4.4 ± 0.4 Hz).

Spin-state selective $^{13}C^\alpha$ relaxation dispersions (magnetization of the form $2C_T^\alpha H|\alpha\rangle$ and $2C_T^\alpha H|\beta\rangle$, where C^α and H are the one-bond scalar coupled $^{13}C^\alpha$ and $^1H^\alpha$ spins, "T" denotes transverse magnetization and $|\kappa\rangle$ is the $\{\alpha,\beta\}$ spin state of $^1H^\alpha$) were recorded on Varian Inova spectrometers operating at 14.1 T (600 MHz) (cryogenically cooled probe) and 18.8 T (room temperature probe), 25 °C. Dispersion curves were obtained using a pulse scheme described in the text. The data was supplemented by profiles that measure the relaxation of in-phase $^{13}C^\alpha$ magnetization using a sequence very similar to that described previously[31] (available from the authors upon request). Fifteen values of ν_{CPMG} between 33 and 933 Hz ($T_{relax} = 30$ ms) were recorded for the spin-state selective measurements along with two duplicate points, at magnetic fields of both 14.1 and 18.8 T, while 13 (16) values of ν_{CPMG} were obtained to define the in-phase $^{13}C^\alpha$ dispersions at 14.1(18.8) T (two duplicate measurements).

$^1H^\alpha-^{13}C^\alpha$ RDCs of the SH3 domain with fully bound Ark1p peptide were derived from IPAP experiments[34,35] recorded on samples with and without alignment media. Values of $J_{eff} = J_{C\alpha H\alpha} + D_{C\alpha H\alpha}$ (aligned) and $J_{eff} = J_{C\alpha H\alpha}$ (no alignment) were obtained, where $J_{C\alpha H\alpha}$ and $D_{C\alpha H\alpha}$ are the one-bond $^1H^\alpha-^{13}C^\alpha$ scalar and dipolar couplings, respectively.

Data Analysis. Data sets were processed with the NMRPipe program,[36] signal intensities quantified with the Function and Data Analysis program, FuDA (available from flemming@pound.med.utoronto.ca), and spectra were visualized using the SPARKY program.[37] Relaxation dispersion profiles, $R_{2,eff}(\nu_{CPMG})$ vs. ν_{CPMG}, were calculated as $R_{2,eff}(\nu_{CPMG}) = -\ln(I(\nu_{CPMG})/I_0)/T_{relax}$, where $I(\nu_{CPMG})$ is the peak intensity for different ν_{CPMG} values and I_0 is the peak intensity obtained when the CPMG block is omitted.[38] Here $\nu_{CPMG} = 1/(4\tau_{CP})$, where $2\tau_{CP}$ is the interval between successive 180° refocusing pulses during the CPMG element. Uncertainties in $R_{2,eff}(\nu_{CPMG})$ values, $\Delta R_{2,eff}^{exp}$, were chosen to be the maximum of {errors calculated on the basis of duplicate measurements, 2% of $R_{2,eff}(\nu_{CPMG})$, 0.4 s^{-1}}.

Relaxation dispersion data were analyzed using in-house written software (available upon request) under the assumption of a two-site chemically exchanging system, $A \underset{k_{BA}}{\overset{k_{AB}}{\rightleftharpoons}} B$. Best-fit model parameters that describe the chemically exchanging system, i.e., the rate of chemical exchange, $k_{ex} = k_{AB} + k_{BA}$, the population of the invisible state, $p_B = k_{AB}/k_{ex}$, the chemical shift difference between states, $\Delta\varpi = \varpi_A - \varpi_B$ (ppm), the difference in residual dipolar couplings of the two states $\Delta D = D_A - D_B$, and intrinsic exchange-free relaxation rates, $R_{2,eff}(\infty) = \lim_{\nu_{CPMG}\to\infty} R_{2,eff}(\nu_{CPMG})$ (assumed equivalent in the two states) were determined as the model parameters that minimize the target function,

$$\chi^2(\zeta) = \sum \left(\frac{R_{2,eff}^{calc}(\zeta) - R_{2,eff}^{exp}}{\Delta R_{2,eff}^{exp}} \right)^2 \quad (1)$$

Here, ζ is a vector of the adjustable model parameters that includes both global (k_{ex}, p_B) and residue specific ($\Delta\varpi$, ΔD, $R_{2,eff}(\infty)$) values, $R_{2,eff}^{exp}$ is the measured effective relaxation rate, $R_{2,eff}^{calc}(\zeta)$ is an effective relaxation rate calculated from the model parameters as described below, and the sum is over all experimental data points. The

(30) Haynes, J.; Garcia, B.; Stollar, E. J.; Rath, A.; Andrews, B. J.; Davidson, A. R. *Genetics* **2007**, *176*, 193–208.
(31) Hansen, D. F.; Vallurupalli, P.; Lundstrom, P.; Neudecker, P.; Kay, L. E. *J. Am. Chem. Soc.* **2008**, *130*, 2667–2675.
(32) Lundstrom, P.; Teilum, K.; Carstensen, T.; Bezsonova, I.; Wiesner, S.; Hansen, D. F.; Religa, T. L.; Akke, M.; Kay, L. E. *J. Biomol. NMR* **2007**, *38*, 199–212.
(33) Yang, D.; Kay, L. E. *J. Biomol. NMR* **1999**, *13*, 3–10.
(34) Ottiger, M.; Delaglio, F.; Bax, A. *J. Magn. Reson.* **1998**, *131*, 373–378.
(35) Yang, D.; Nagayama, K. *J. Magn. Reson. Ser. A* **1996**, *118*, 117–121.
(36) Delaglio, F.; Grzesiek, S.; Vuister, G. W.; Zhu, G.; Pfeifer, J.; Bax, A. *J. Biomol. NMR* **1995**, *6*, 277–293.
(37) Kneller, D.; Kuntz, I. *J. Cell. Biochem.* **1993**, *Suppl. 17C*, 254.
(38) Mulder, F. A. A.; Skrynnikov, N. R.; Hon, B.; Dahlquist, F. W.; Kay, L. E. *J. Am. Chem. Soc.* **2001**, *123*, 967–975.

Levenberg−Marquardt algorithm of Numerical Recipes in C++ (3rd edition[39]) was used for least-squares minimization of the target function χ^2.

Intensities and rates, $I^{calc}(\zeta)$ and $R_{2,eff}^{calc}(\zeta)$, were calculated by evolving the relevant density elements over the CPMG part of the appropriate pulse scheme (Figures 1 or 4 of the text), including off-resonance effects of pulses and summing the results over the complete phase cycle considered experimentally. In the case of spin-state selective experiments the effect of ^{1}H spin flips is explicitly taken into account using experimentally derived spin flip rates, as described previously.[19] In the analysis of the spin-state selective experiments a 13-element basis is considered that includes the unity operator, E, and six elements $\{2C_XH^{|\beta\rangle}, 2C_YH^{|\beta\rangle}, 2C_ZH^{|\beta\rangle}, 2C_XH^{|\alpha\rangle}, 2C_YH^{|\alpha\rangle}, 2C_ZH^{|\alpha\rangle}\}$ for each of the two chemically exchanging sites, where $C,H = \{^{13}CO,^1HN\}$ or $\{^{13}C^\alpha,^1H^\alpha\}$, depending on the experiment. In this basis ^{1}H spin flips couple magnetization of the form $2C_jH^{|\alpha\rangle}$ and $2C_jH^{|\beta\rangle}$ (see text). In the analysis of relaxation dispersion profiles derived from either in-phase ^{13}CO or $^{13}C^\alpha$ (with respect to the relevant coupled protons) a simple seven-element basis was used in simulations, consisting of E, and $\{C_X, C_Y, C_Z\}$ for each of the chemically exchanging sites. Evolution of the basis elements proceeds according to a system of coupled equations that follows directly from eq [23] of Helgstrand et al.,[40] modified to include two-site chemical exchange as described previously,[41] with the multiple-quantum terms that are not of interest presently removed. At the end of the simulation period coherences of the form $2C_zH^{|\beta\rangle}$ from each of the two chemically exchanging sites (corresponding to the coherences retained experimentally) are used to calculate the final intensity, $I^{calc}(\zeta)$ as a weighted average. The coefficients used in the weighting are those used to generate the eigenvector of the two-site exchange matrix whose eigenvalue (imaginary part) is closest to the frequency of the major state in the absence of exchange, ω_A. Finally, the effective relaxation rate is calculated as $R_{2,eff}^{calc}(\zeta) = -\ln(I^{calc}(\zeta)/I_0)/T_{relax}$, as for the experimentally derived rates. $^{13}C^\alpha-^{15}N$ ($^{13}CO-^{15}N$) scalar couplings evolve during the τ_{CP} delays in the $^{13}C^\alpha$ (^{13}CO) constant-time CPMG relaxation experiments (see Figures 1 and 4), potentially complicating analysis; however, it was shown previously[42] that the errors introduced by $^{13}C-^{15}N$ scalar couplings are negligibly small for T_{relax} values used here (<1%). These couplings were therefore not taken into account in any of the fits.

In the analysis of a given class of dispersion experiment ($^{13}C^\alpha$ or ^{13}CO), dispersion profiles for all residues obtained at two static magnetic field strengths were analyzed together, using common kinetics parameters k_{ex} and p_B, whereas the parameters $\Delta\varpi$, ΔD, and $R_{2,eff}(\infty)$ were adjusted separately for each residue. Standard errors of all the adjustable model parameters were calculated from the covariance matrix of the least-squares fit.[39] Relaxation dispersions were excluded if the two-site chemical exchange model did not generate statistically significant improvements over a model with no chemical exchange (constant $R_{2,eff}$) at the 98% confidence level. In the case of the ^{13}CO sample, 38 out of 50 dispersions showed significant chemical exchange ($p < 0.02$), whereas 24 out of the 42 $^{13}C^\alpha$ dispersion profiles were retained (note that six Leu, three Ile, and three Val residues were excluded due to the labeling scheme employed, see above). Relaxation dispersions were also excluded if the standard error of $|\Delta D|$ was larger than 5 Hz, leaving finally 28 ^{13}CO and 17 $^{13}C^\alpha$ dispersions for analysis.

A prerequisite for obtaining dipolar couplings probing the excited-state is to first obtain the signs of $\Delta\varpi$. Although this information is not available from analysis of relaxation dispersion data sets, it can be obtained by the method of Skrynnikov et al.,[43] as has been described previously for the analysis of ^{13}CO and $^{13}C^\alpha$ dispersion data sets recorded in isotropic media.[31] Briefly, signs of $\Delta\varpi(^{13}CO)$ were obtained by measuring ^{13}CO chemical shifts in $^{13}CO-^1HN$ HSQC- and HMQC-type spectra at both 11.7 and 18.8 T; changes in peak positions in the four experiments provide the desired sign information. Signs of $\Delta\varpi(^{13}C^\alpha)$ were obtained from a comparison of $^1H^\alpha-^{13}C^\alpha$ HSQC spectra recorded at 11.7 and 18.8 T. As described previously,[31] the sign of $\Delta\varpi$ can be determined accurately via this method as long as $|\Delta\varpi| > 0.1$ ppm.

Results and Discussion

Choice of Exchanging System. We have chosen an exchanging system that involves ligand binding, $P + L \underset{k_{off}}{\overset{k_{on}}{\rightleftharpoons}} PL$, because the system is readily manipulated through the addition of ligand for cross-validation of measurements. For example, at low $[L_{TOTAL}]/[P_{TOTAL}]$ ($\approx 5\%$), only the P state is visible in NMR spectra, whereas the bound conformation, PL, is the "excited", invisible state that is probed by spin-state relaxation dispersion CPMG measurements. Extracted dipolar couplings (see below) that are obtained in this manner for PL can then be compared with those that are measured using conventional "direct" experiments recorded on a sample where saturating amounts of ligand are added so that PL is "transformed" into the visible ground state. The system used here is one that we have exploited in previous work[19] where P is the Abp1p SH3 domain and L is a 17 residue target peptide that dissociates with a K_D of 0.55 μM, with $k_{ex} = k_{on}[L] + k_{off}$ values that are within the exchange window that is amenable for the CPMG class of experiment. Electrostatics are an important component to the present interaction since the Abp1p SH3 domain has a net negative charge of 12 and the Ark1p peptide a net positive charge of 7 at pH = 7. Because phage particles (that are highly charged) are used for alignment, the difference in charge between P and PL leads to large differences in their alignment frames. Exchange between free and bound protein results, therefore, in a modulation of alignment frames and hence of dipolar couplings. It is worth noting, however, that in general changes in alignment properties between the exchanging states are not a prerequisite for the success of the approach. Indeed, what is of interest are the structural changes between states and these also produce time-dependent modulations of anisotropic interactions, even in the absence of differences in alignment; such changes can be quantified by the experiments described below.

Measurement of Two-Bond ^{1}HN−^{13}CO RDCs. The HNCO-CPMG based pulse scheme for measuring $^2D_{HN,CO}$ is shown in Figure 1. The goal is to create ^{13}CO transverse magnetization (residue i) at point f that is correlated with ^1HN (residue $i+1$) in either the α (experiment 1) or β (experiment 2) spin-state;

(39) Press, W. H.; Flannery, B. P.; Teukolsky, S. A.; Vetterling, W. T. *Numerical Recipes in C.*; Cambridge University Press: Cambridge, 1988.
(40) Helgstrand, M.; Hard, T.; Allard, P. *J. Biomol. NMR* **2000**, *18*, 49–63.
(41) Hansen, D. F.; Yang, D.; Feng, H.; Zhou, Z.; Wiesner, S.; Bai, Y.; Kay, L. E. *J. Am. Chem. Soc.* **2007**, *129*, 11468–11479.
(42) Ishima, R.; Baber, J.; Louis, J. M.; Torchia, D. A. *J. Biomol. NMR* **2004**, *29*, 187–198.
(43) Skrynnikov, N. R.; Dahlquist, F. W.; Kay, L. E. *J. Am. Chem. Soc.* **2002**, *124*, 12352–12360.
(44) Levitt, M.; Freeman, R. *J. Magn. Reson.* **1978**, *33*, 473–476.
(45) Geen, H.; Freeman, R. *J. Magn. Reson.* **1991**, *93*, 93–141.
(46) Gullion, T.; Baker, D. B.; Conradi, M. S. *J. Magn. Reson.* **1990**, *89*, 479–484.
(47) Kupce, E.; Freeman, R. *J. Magn. Reson., Ser. A.* **1995**, *115*, 273–276.
(48) Hansen, D. F.; Vallurupalli, P.; Kay, L. E. *J. Phys. Chem. B* **2007**, *112*, 5898–5904.
(49) Kay, L. E.; Keifer, P.; Saarinen, T. *J. Am. Chem. Soc.* **1992**, *114*, 10663–10665.
(50) Schleucher, J.; Sattler, M.; Griesinger, C. *Angew. Chem., Int. Ed. Engl.* **1993**, *32*, 1489–1491.
(51) Marion, D.; Ikura, M.; Tschudin, R.; Bax, A. *J. Magn. Reson.* **1989**, *85*, 393–399.
(52) Nietlispach, D. *J. Biomol. NMR* **2005**, *31*, 161–166.

then differences in spin-state selective relaxation dispersion profiles report directly on changes in $^1HN-^{13}CO$ dipolar couplings between exchanging states as described below. In what follows, a brief description of the pulse scheme is presented.

Starting from both ^1HN and ^{15}N steady state polarization, transverse ^{15}N magnetization is created that subsequently evolves for a period of $2\tau_b = 1/(4|J_{NH}|)$ between points *a* and *b*, where J_{NH} is the one-bond $^1H-^{15}N$ scalar coupling constant (≈ -93 Hz). The phase ϕ_1 of the ^{15}N 90° pulse is set to 45° so that immediately after the second ^{15}N 90° pulse at point *b* and the ensuing gradient (g5), nitrogen magnetization that is coupled to the $^1HN^{|\beta\rangle}$ spin-state is selected preferentially (^{15}N magnetization coupled to $^1HN^{|\alpha\rangle}$ is dephased). For molecules dissolved in isotropic solution and for a uniform value of J_{NH} the selection is (close to) perfect. However, under conditions of residual alignment evolution proceeds due to *both* scalar and dipolar $^1H-^{15}N$ couplings so that the ratio of transverse ^{15}N magnetization (N_T) selected in the α and β spin-states ($N_THN^{|\alpha\rangle}/N_THN^{|\beta\rangle}$) is given by $\tan[(\pi D_{NH})/(4J_{NH})]$. During the period extending from *c* to *d*, ^{15}N magnetization evolves due to the one-bond $^{15}N-^{13}CO$ scalar (and dipolar) coupling. Simultaneous ^{13}CO and ^{15}N pulses are applied to minimize the deleterious effects from chemical exchange that lead to signal attenuation, as described previously.[31] As indicated in Figure 1 a train of 32 such pulses are applied during an interval of duration 2T, suppressing contributions from exchange events that take place with frequencies on the order of 8/T or slower. Evolution due to $^{15}N-^{13}CO$ scalar coupling continues for an additional interval of $2\tau_b$ (*d* to *e*). Most important is that during this period there is an additional filter step that suppresses ^{15}N magnetization coupled to ^1HN in the α spin-state yet again, leading to a net effective relative attenuation of $r = \tan^2[(\pi D_{NH})/(4J_{NH})]$. Note that during the lengthy transfer period between *c* and *d* the magnetization of interest is coupled to $^1HN^{|\beta\rangle}$, corresponding to the slowly relaxing TROSY component[13] and that any residual nitrogen magnetization coupled to $^1HN^{|\alpha\rangle}$ ($r \leq 7\%$ for $|D_{NH}| \leq 30$ Hz) will be attenuated further due to fast relaxation. Up to point *e* in the sequence, the magnetization transfer can be summarized as

$$H_Z, N_Z \rightarrow N_THN^{|\beta\rangle} \rightarrow N_ZCO_ZHN^{|\alpha\rangle} \quad (2)$$

where the subscripts *T* and *Z* denote transverse and Z-magnetization, respectively. It is important to emphasize that between points *c* and *d* nitrogen magnetization is coupled to the β ^1HN spin-state (TROSY), but that the ^1H 180° pulse in the interval between *d* and *e* converts $^1HN^{|\beta\rangle}$ to $^1HN^{|\alpha\rangle}$.

Central to the experiment is the constant-time CPMG-based element between points *f* and *g*. Separate dispersion profiles are recorded for carbonyl magnetization coupled to $^1HN^{|\alpha\rangle}$ or $^1HN^{|\beta\rangle}$, and the relevant starting coherences (point *f*) are $4CO_XN_ZHN^{|\alpha\rangle}$ and $4CO_XN_ZHN^{|\beta\rangle}$, respectively (referred to in what follows as CO-$HN^{|\alpha\rangle}$ and CO-$HN^{|\beta\rangle}$ dispersions). In the latter case an additional ^1H 180° pulse (red) must be applied that "converts" $4CO_XN_ZHN^{|\alpha\rangle}$ (point *e*) to $4CO_XN_ZHN^{|\beta\rangle}$ prior to the CPMG pulse train (see eq 2). During the CPMG interval, a variable number of ^{13}CO refocusing pulses are applied at a frequency $\nu_{CPMG} = 1/(4\tau_{CP})$, where $2\tau_{CP}$ is the time between the centers of successive 180° pulses. It is straightforward to show that during the delays between pulses magnetization described by terms of the form $4CO_XN_ZHN^{|\beta\rangle}$ and $4CO_XN_ZHN^{|\alpha\rangle}$ evolves as $\nu_{CO} + J_{CO,HN}/2 + D_{CO,HN}/2$ and $\nu_{CO} - J_{CO,HN}/2 - D_{CO,HN}/2$, respectively, where we have included explicitly only those contributions from $^{13}CO-^1HN$ couplings. In addition, there are further modulations from $^{15}N-^{13}CO$ couplings but these will not interfere with the extraction of $D_{CO,HN}$ values since individual ^{15}N spin-states are not selected in the experiment (see results below). Thus, for a system exchanging between two states, $A \rightleftharpoons B$ (A is the major state), the dispersion experiments are sensitive to an "effective frequency difference" between the exchanging states that is given by $\Delta\nu + 0.5\Delta D_{CO,HN}$ (CO-$HN^{|\beta\rangle}$ dispersions) and $\Delta\nu - 0.5\Delta D_{CO,HN}$ (CO-$HN^{|\alpha\rangle}$ dispersions) where $\Delta\nu = \nu_A - \nu_B$, $\Delta D_{CO,HN} = D^A_{CO,HN} - D^B_{CO,HN}$ and we have assumed that $J_{CO,HN}$ is the same in both states. It is worth noting that in the case of the N-$HN^{|\beta\rangle}$, N-$HN^{|\alpha\rangle}$ dispersions considered previously,[19] the frequency differences are given by $\Delta\nu - 0.5\Delta D_{N,HN}$ (N-$HN^{|\beta\rangle}$ dispersions) and $\Delta\nu + 0.5\Delta D_{N,HN}$ (N-$HN^{|\alpha\rangle}$ dispersions), exactly the reverse. This reflects the sign difference between ^{15}N and ^{13}CO gyromagnetic ratios.

Finally, at the completion of the CPMG interval (point *g*), ^{15}N chemical shift is recorded (in a semi constant-time manner) and magnetization subsequently transferred back to ^1HN for observation, following an enhanced sensitivity-based TROSY scheme that was described by Nietlispach.[52] Because sensitivity is maximal when ^{15}N magnetization is transferred as the TROSY component, a ^1H 180° pulse must applied at point *g* (blue pulse) in the case where CO-$HN^{|\alpha\rangle}$ dispersions are measured.

As described above, pairs of experiments are recorded monitoring carbonyl magnetization coupled to either $^1HN^{|\alpha\rangle}$ or $^1HN^{|\beta\rangle}$ spin-states and the accuracy of the extracted dipolar couplings depends, therefore, on preserving these spin-states during the constant-time CPMG interval. Relaxation from external protons leads to spin-state exchange and this can be minimized very significantly through the use of deuterated protein samples, as done here. However, amide protons still remain and spin flips are thus not fully quenched. Their deleterious effect can be appreciated by considering a simple coupled $^{13}CO-^1HN$ spin system that is not in chemical exchange and noting that the evolution of transverse ^{13}CO magnetization, CO_T, coupled to either $^1HN^{|\alpha\rangle}$ ($M_{CO_THN^{|\alpha\rangle}}$) or $^1HN^{|\beta\rangle}$ ($M_{CO_THN^{|\beta\rangle}}$), can be approximated by,

$$\frac{d}{dt}\begin{pmatrix} M_{CO_THN^{|\alpha\rangle}} \\ M_{CO_THN^{|\beta\rangle}} \end{pmatrix} = -\begin{pmatrix} \rho_\alpha + k_\alpha & -0.5R_{1S,H} \\ -0.5R_{1S,H} & \rho_\beta + k_\beta \end{pmatrix}\begin{pmatrix} M_{CO_THN^{|\alpha\rangle}} \\ M_{CO_THN^{|\beta\rangle}} \end{pmatrix} \quad (3)$$

where ρ_α, ρ_β are the decay rates of $M_{CO_THN^{|\alpha\rangle}}$ and $M_{CO_THN^{|\beta\rangle}}$ in the absence of external protons, $k_\alpha = 0.5R_{1S,H} - i(\omega - \pi D_{CO,HN} - \pi J_{CO,HN})$, $k_\beta = 0.5R_{1S,H} - i(\omega + \pi D_{CO,HN} + \pi J_{CO,HN})$, $R_{1S,H}$ is the selective ^1HN longitudinal relaxation rate that very well approximates twice the amide proton spin flip rate,[53] and $M = M_X + iM_Y$, where M_X and M_Y are the *X* and *Y* components of magnetization. Note that each of $M_{CO_THN^{|\alpha\rangle}}$ and $M_{CO_THN^{|\beta\rangle}}$ evolves at discrete frequencies and that spin flips interconvert the magnetization components. This situation is analogous to a two-site chemical exchange process and, depending on the initial conditions (*i.e.*, the relative amounts of $M_{CO_THN^{|\alpha\rangle}}$ and $M_{CO_THN^{|\beta\rangle}}$), spin flips can lead to artificial dispersion profiles that reflect spin, not chemical, exchange events. As first shown by Loria et al.[54] it is possible to insert an element in the middle of the CPMG interval that inverts transverse magnetization associated with either the $^1HN^{|\alpha\rangle}$ or the $^1HN^{|\beta\rangle}$ spin-state (not both) that results in a very efficient suppression of these effects. Here we have taken a different route that involves selection of

(53) Goldman, M. *J. Magn. Reson.* **1984**, *60*, 437–452.
(54) Loria, J. P.; Rance, M.; Palmer, A. G. *J. Biomol. NMR* **1999**, *15*, 151–155.

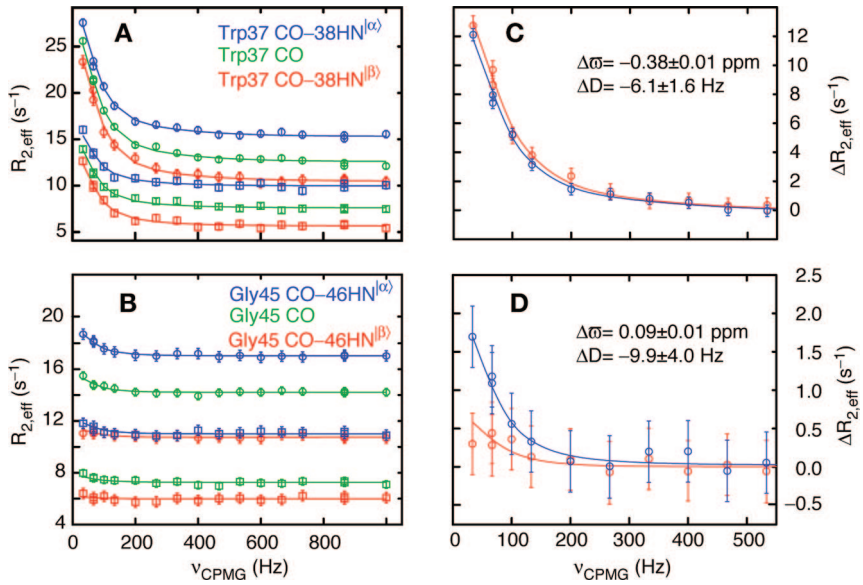

Figure 2. ^{13}CO relaxation dispersion profiles from Trp37 (A and C) and Gly45 (B and D) of Abp1p SH3, 7% Ark1p peptide, 25 °C, Pf1 phage, recorded at static magnetic fields of 18.8 T (O) and 11.7 T (□). Blue (red) data points indicate dispersion profiles obtained by measuring the relaxation of $4CO_TN_ZHN^{|\alpha\rangle}$ ($4CO_TN_ZHN^{|\beta\rangle}$), while transverse relaxation rates of $2CO_TN_Z$, obtained with a pulse scheme described previously,[31] are in green. Continuous lines indicate least-squares fits of a two-site chemical exchange model to the data shown (see Material and Methods). Figures 2C and 2D show dispersion curves for Trp37 and Gly45 recorded at 18.8 T where the exchange-free transverse relaxation rate, $R_{2,eff}(\infty) = \lim_{\nu_{CPMG}\to\infty}[R_{2,eff}(\nu_{CPMG})]$, has been subtracted from the effective relaxation rate ($\Delta R_{2,eff} = R_{2,eff} - R_{2,eff}(\infty)$) to clarify the differences in sizes of the spin-state selective dispersion profiles.

magnetization that is coupled to only $^1HN^{|\alpha\rangle}$ or $^1HN^{|\beta\rangle}$ at the start of the CPMG interval, with the other component quenched, as described above. That this minimizes the effect of spin flips can be seen in a straightforward manner from eq 3 by noting, for example, that if $CO_THN^{|\alpha\rangle}$ is selected, that is if $M_{CO_THN^{|\beta\rangle}}(0) = 0$, then the initial decay of $M_{CO_THN^{|\alpha\rangle}}$ proceeds exponentially with a rate of $\rho_\alpha + k_\alpha$ and spin flips do not interfere with the extraction of accurate exchange parameters. Experiments on the system studied here using pulse schemes very similar to Figure 1 (but without the CPMG train) show that essentially only one of the two components is present at the start of the CPMG element, $r < 5\%$ (see above) and simulations for the system described by eq [3] with $r = 0.05$, $D_{CO,NH} + J_{CO,NH} = 20$ Hz, $R_{1S,H} = 11$ s^{-1} and $T_{relax} = 40$ ms (see Figure 1) establish that dispersion curves, $R_{2,eff}(\nu_{CPMG})$, are obtained with $\Delta = R_{2,eff}(\nu_{CPMG} = 25\text{ Hz}) - R_{2,eff}(\nu_{CPMG} = 1000\text{ Hz}) < 0.3$ s^{-1}. This represents an upper bound for Δ because $R_{1S,H} = 11$ s^{-1} is the largest spin flip rate measured experimentally ($\langle R_{1S,H}\rangle = 1.8 \pm 1.0$ s^{-1}) and measured values of $D_{CO,NH} + J_{CO,NH}$ are ≤ 20 Hz (larger values increase Δ). Recall that $R_{2,eff}(\nu_{CPMG})$ profiles are ideally flat for a system that is not in chemical exchange. Errors of 0.3 s^{-1} are well within the noise and can be tolerated without problem.

Figure 2A, B presents relaxation dispersion profiles measured for Trp37 and Gly45 of the Abp1p SH3 domain with 7% peptide, 25 °C (see Materials and Methods) at 11.7 T (bottom 3 curves in each plot, squares) and 18.8 T (circles). CO-$HN^{|\alpha\rangle}$ (blue) and CO-$HN^{|\beta\rangle}$ (red) dispersions are recorded, along with profiles that are not spin-state selective (green) using a pulse scheme that has been described previously[31]. The sets of dispersion curves recorded at 11.7 and 18.8 T are offset, reflecting the fact that the dominant relaxation mechanism for transverse carbonyl magnetization is CSA that scales quadratically with magnetic field. Differences in $R_{2,eff}(\infty)$ between "spin-state selective" profiles recorded at a single field are due to the interference effect between ^{13}CO CSA and ^{1}HN−^{13}CO dipolar interactions so that $\rho_\alpha > \rho_\beta$. The spin-state independent profile

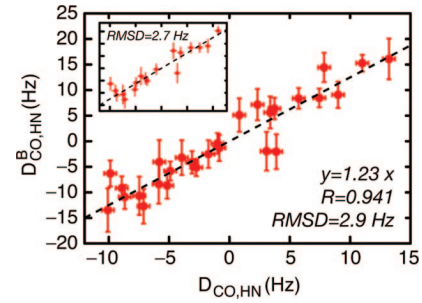

Figure 3. Correlation plot of ^{1}HN−^{13}CO RDCs of the invisible minor state, *PL*, ($D^B_{NH,CO}$) measured on a sample with 7% *L* using the CPMG method of Figure 1 (*y* axis) vs. dipolar couplings obtained through direct measurements on a fully bound sample, $D_{CO,HN}$ (*x* axis). Error bars, corresponding to one standard deviation, are indicated. Main figure includes all values that could be quantified irrespective of the magnitude of $\Delta\varpi$. (Inset) Data from carbonyl carbons for which the sign of $\Delta\varpi$ was determined by the method of Skyrnnikov et al.[43] ($|\Delta\varpi| > 0.1$ ppm). The dashed line is the best-fit line to the data, ($y = 1.23x$), *R* is the coefficient of linear correlation and rmsd is the root-mean-square-deviation of the data points to the best-fit line. The slope of the best-fit line is different from one since less Pf1 phage was used for the direct measurements ($D_{CO,HN}$) than for the indirect CPMG measurements ($D^B_{NH,CO}$), which reflects the difficulty in preparing samples with identical concentrations of alignment media.

is derived from magnetization with an intrinsic relaxation rate of approximately $(\rho_\alpha + \rho_\beta)/2$ and thus lies approximately midway between the other curves. Shown also in the figure are the best fits of the relaxation dispersion profiles using an in-house written program that has been described both in Materials and Methods and in a separate publication[19]. As discussed in Materials and Methods a single global fit of the data to a 2-site chemical exchange process was performed, with 28 sets of profiles of the types shown in the figure (recorded at two static magnetic fields) analyzed simultaneously to extract $|\Delta D_{CO,HN}|$ values. Figure 2C, D shows expansions of the spin-state selective dispersion profiles recorded at 18.8 T, "normalized" to have the same $R_{2,eff}(\infty)$ (see legend), emphasizing the (small) differences that arise from $\Delta D_{CO,HN} \neq 0$.

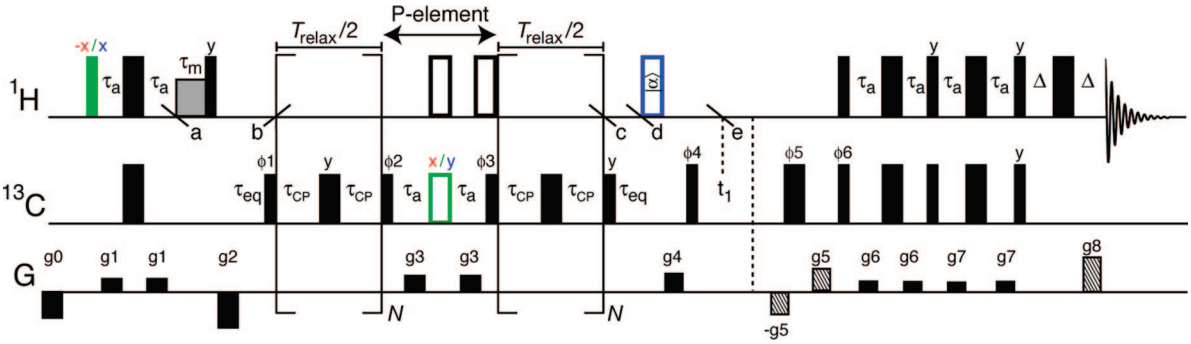

Figure 4. Spin-state selective pulse scheme for the measurement of $^{13}C^{\alpha}$ TROSY ($2C_TH^{|\beta\rangle}$; red) and anti-TROSY ($2C_TH^{|\alpha\rangle}$; blue) constant-time CPMG relaxation dispersion profiles in protein systems undergoing millisecond time-scale exchange. All ^{1}H and ^{13}C 90° (180°) rf pulses are shown as narrow (wide) black bars and are applied at the highest possible power level, with the exception of the ^{13}C refocusing pulses of the CPMG element along with the 90° sandwiching pulses, which are applied at a slightly lower power level (~15 kHz). Composite 180° pulses ($90_x-180_y-90_x$) are represented by open rectangles. A Messerlie[58] spin-lock purge element is applied at point *a* to remove residual water magnetization. All pulse phases are assumed to be *x*, unless indicated otherwise. *N* can be any whole number. The ^{1}H rf carrier is placed on the residual water signal, whereas the ^{13}C rf carrier is positioned in the center of the $^{13}C^{\alpha}$ region (~56 ppm). The composite 180° proton pulse at point *d* is applied only when recording relaxation dispersion profiles for magnetization of the form $2C_TH^{|\alpha\rangle}$, converting $2C_TH^{|\alpha\rangle}$ *to* $2C_TH^{|\beta\rangle}$ *at d*; in all experiments, $2C_TH^{|\beta\rangle}$ is selected by a sensitivity enhancement scheme.[52] The phase cycling used is (Varian): $\phi1 = \{x,-x\}$, $\phi2 = 2\{y\},2\{-y\}$, $\phi3 = 2\{x\},2\{-x\}$, $\phi4 = \{x\}$, $\phi5 = 2\{x\},2\{-x\},2\{y\},2\{-y\}$, $\phi6 = x$, receiver $= 2\{x,-x\},2\{-x,x\}$. Sensitivity enhanced quadrature detection in the indirect dimension is obtained by recording a second data set with $\phi6 = \phi6 + \pi$ and inverting the sign of gradient *g*5 for each t_1 increment.[49,50] In addition, phase $\phi4$ is incremented along with the receiver by π for each complex t_1 point.[51] The delays used are $\tau_a = 1.79$ ms, $\tau_m = 1.0$ ms, $\tau_{eq} = (2-3)/(k_{ex}) \approx 5$ ms, where the τ_{eq} delay ensures equilibrium populations at the start and end of the CPMG relaxation element. Gradient strengths G/cm (length in ms) are: $g0 = -15(1)$, $g1 = 5(0.4)$, $g2 = -30(1)$, $g3 = 8(0.3)$, $g4 = 10(0.5)$, $g5 = 15(0.4)$, $g6 = 4(0.2)$, $g7 = 2.5(0.8)$, $g8 = 29.3(0.1)$. A 180° nitrogen pulse is applied at point *e* (in the middle of the t_1 evolution period) to refocus scalar couplings between $^{13}C^{\alpha}$ and ^{15}N, when the protein is labelled with ^{15}N. The construction of the P-element (center of the CPMG scheme) is as described previously.[19]

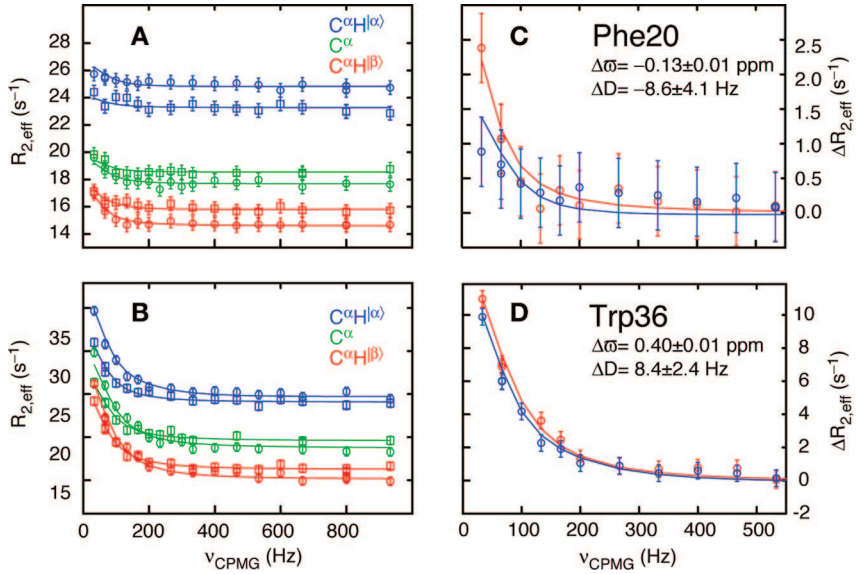

Figure 5. $^{13}C^{\alpha}$ TROSY (red; corresponding to magnetization of the form, $2C_TH^{|\beta\rangle}$), in-phase (green; C_T) and anti-TROSY (blue; $2C_TH^{|\alpha\rangle}$) relaxation dispersion profiles for Phe20 (A and C) and Trp36 (B and D) of Abp1p SH3, 7% Ark1p peptide, dissolved in Pf1 phage alignment media, 25 °C and recorded at static magnetic fields of 18.8 T (○) and 14.1 T (□). Continuous lines are least-squares fits (see Materials and Methods) of a two-site model of chemical exchange to the data. (C and D) Dispersion curves recorded at 18.8 T, with the exchange-free transverse relaxation rate, $R_{2,eff}(\infty) = \lim_{\nu_{CPMG}\to\infty}[R_{2,eff}(\nu_{CPMG})]$, subtracted from the effective relaxation rate ($\Delta R_{2,eff} = R_{2,eff} - R_{2,eff}(\infty)$) to clarify the different magnitudes of the relaxation dispersion profiles of $2C_TH^{|\alpha\rangle}$ and $2C_TH^{|\beta\rangle}$ arising from $\Delta D \neq 0$. The magnitude of the dispersions derived from $2C_TH^{|\beta\rangle}$ are larger in both cases since $\Delta\varpi \times \Delta D > 0$.

Values of $D^A_{CO,HN}$ have been measured for the ground (visible) state, *P*, from a pair of 2D spin-state selective HNCO correlation maps connecting ^{13}CO and ^{1}HN chemical shifts of residues *i* and *i*+1 respectively. Correlations of the form ($\nu^A_{CO} + 0.5J_{CO,HN} + 0.5D^A_{CO,HN}$, $\nu^A_{HN} + 0.5J_{NH} + 0.5D^A_{NH}$) (data set 1) or ($\nu^A_{CO} - 0.5J_{CO,HN} - 0.5D^A_{CO,HN}$,$\nu^A_{HN} + 0.5J_{NH} + 0.5D^A_{NH}$) (data set 2) were obtained from which $J_{CO,HN} + D^A_{CO,HN}$ was quantified on a per-residue basis. In principal, experiments could also be recorded in the isotropic phase to measure $J_{CO,HN}$ that would then allow extraction of $D^A_{CO,HN}$. We note, however, that values for $J_{CO,HN}$ are relatively uniform (4.4 ± 0.4 Hz, as measured from 275 well resolved correlations in maltose binding protein[16]) and here we have assumed a constant value of 4.4 Hz so that values of $D^A_{CO,HN}$ could be isolated.

Values of $D^B_{CO,HN}$ have been calculated from $D^A_{CO,HN}$ and $\Delta D_{CO,HN}$. Figure 3 shows an excellent correlation between $D^B_{CO,HN}$ values measured via the CPMG method on a sample where *PL* is the invisible state (7% *PL*, Y axis) and the corresponding values obtained directly from a sample containing saturating amounts of peptide (X axis). A Pearson correlation coefficient, *R*, of 0.94 is obtained, with 78% of the data points within one standard deviation (1σ) of the best-fit line and 93%

of the points within 2σ, consistent with expectations based on a normal distribution of errors. The main figure includes $D^B_{CO,HN}$ values from all residues for which quantifiable dispersions were obtained (see Materials and Methods). As discussed previously relaxation dispersion experiments are not sensitive to the signs of chemical shift differences.[23] However, because profiles have been recorded that report on $|\Delta\nu + 0.5\Delta D_{CO,HN}|$ ($CO-HN^{|\beta\rangle}$ dispersions), on $|\Delta\upsilon - 0.5\Delta D_{CO,HN}|$ ($CO-HN^{|\alpha\rangle}$ dispersions), and on $|\Delta\nu|$ (CO dispersions[31]), the sign of $\Delta D_{CO,HN}$ and hence the value of $D^B_{CO,HN}$ can be obtained if the sign of $\Delta\nu$ is known.[19] In the main figure this sign information has been obtained directly from spectra recorded on *P* and *PL*. By contrast, the sign of $\Delta\nu$ can also be obtained from measurements on the 7% *PL* sample by comparing ^{13}CO peak positions in HSQC- and HMQC-type spectra where ^{13}CO chemical shifts are recorded from single quantum or $^{15}N-^{13}$CO multiple quantum evolution, respectively, as described by Skrynnikov et al.[43] Signs of $\Delta\nu$ and hence of $\Delta D_{CO,NH}$ have been obtained for 18 residues in this manner, leading to accurate values of $D^B_{CO,HN}$, and the correlation of dipolar couplings from these residues only is shown in the inset to the Figure. Note that the slope of 1.23 of the best fit line reflects the fact that approximately 20% more alignment media was added to the sample containing 7% *L* relative to the fully bound protein sample. In the comparison of $D^B_{CO,HN}$ and $D_{CO,HN}$ it is implicitly assumed that dipolar couplings are proportional to the concentration of alignment media (Pf1 phage in this case) (i.e., that only the magnitude of the alignment tensor is affected by the different concentrations of phage). In practice, the orientation and rhombicity of the tensor may also vary slightly, potentially accounting for some of the deviations from the best-fit line of Figure 3. In general, changes in alignment tensor are only important when dipolar couplings from different samples are compared and will, of course, not degrade the structural content of data recorded on a single sample, under one set of alignment conditions.

Measurement of One-Bond $^1H^\alpha-^{13}C^\alpha$ RDCs. $^1H^\alpha-^{13}C^\alpha$ residual dipolar couplings have been shown to be powerful restraints in defining protein structure in solution[55] and methods for measuring these couplings involving quantification in either the time domain[56] or frequency domain[57] have been proposed. To measure such couplings in invisible, excited states we have made use of a pulse sequence that is analogous to one that was proposed for quantifying $^1H-^{15}N$ RDCs in the excited state,[19] Figure 4.

Here RDCs are measured from spin-state selective relaxation dispersion profiles, in this case that report on the evolution of $^{13}C^\alpha$ transverse magnetization (between *b* and *c*) that is coupled to either α or β $^1H^\alpha$ spin-states (dispersion profiles denoted as $C^\alpha H^{|\alpha\rangle}$and $C^\alpha H^{|\beta\rangle}$, respectively). An Abp1p SH3 domain sample was prepared with the C^α position ^{13}C labeled, as described previously[31] and in Materials and Methods, and 7% peptide was added. Ideally, a sample with protonation confined to the H^α position is desired, so that spin flips can be minimized, but the generation of such samples is not possible at present in our laboratory. Thus, a fully protonated sample was prepared and dissolved in D_2O, so that at a minimum $^1HN-^1H^\alpha$ dipolar

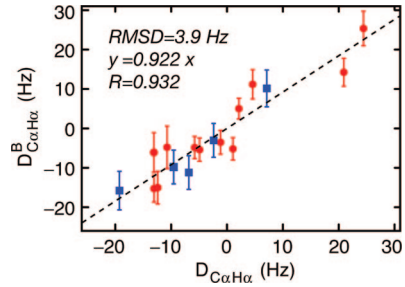

Figure 6. Correlation plot of $^1H^\alpha-^{13}C^\alpha$ RDCs of the invisible minor state, *PL*, ($D^B_{C\alpha,H\alpha}$) measured on a sample with 7% *L* using the CPMG method of Figure 4 (Y axis) vs. dipolar couplings obtained via a direct IPAP[34,35] measurement on a fully bound sample, $D_{C\alpha,H\alpha}$ (X axis). The best-fit line to the data is shown with dashes ($y = 0.922x$), *R* is the coefficient of linear correlation and rmsd is the root-mean square deviation of the points to the best-fit line. The slope of the best-fit line deviates from one because the sample used for the CPMG measurements had slightly less alignment media than the corresponding sample on which the IPAP measurements were made. Points shown with red circles show dipolar coupling values where the sign of $\Delta\varpi$ was obtained using the method of Skrynnikov et al.[43] (see Materials and Methods). Points shown as blue squares correspond to cases where $|\Delta\varpi| < 0.1$ ppm so that the sign of $\Delta\varpi$ was obtained directly from chemical shifts recorded on 7% and 100% bound samples.

interactions are eliminated. The effects of spin flips have been minimized by insertion of a P-element between points *b* and *c* in the figure[19,54] and are additionally taken into account in fits of the dispersion data (also the case for $^1HN-^{13}$CO dispersions), as described previously.[19]Notably, measured values for the cross-relaxation rate between $C^\alpha H^{|\alpha\rangle}$ and $C^\alpha H^{|\beta\rangle}$, $0.5(\rho(2H^\alpha_Z C^\alpha_Z)-\rho(C^\alpha_Z))$, are less than 3.5 s^{-1}, with an average value of 1.5 ± 0.7 s^{-1}, and are on average only a factor of 1.7 larger than the corresponding values measured for the spin flip rate of amide protons in a highly deuterated SH3 domain sample.

Figure 5A, B shows dispersion profiles obtained for residues Phe20 (A) and Trp36 (B) recorded at 14.1 T (squares) and 18.8 T (circles), 25 °C. The top and bottom pairs of dispersion profiles are derived from evolution of $^{13}C^\alpha$ transverse magnetization, $C^\alpha_T H^{|\alpha\rangle}$(blue) and $C^\alpha_T H^{|\beta\rangle}$ (red), during the constant-time CPMG interval, respectively. Not unexpectedly, the anti-TROSY component (blue) relaxes most efficiently at 18.8 T, while the TROSY (red) component relaxes most slowly at this field. The pair of curves in the middle were recorded using a previously published pulse scheme[31] in which in-phase $^{13}C^\alpha$ magnetization evolves during the entire CPMG pulse train. Figure 5C, D shows expanded regions of the spin-state selective dispersion profiles for Phe20 (C) and Trp36 (D) recorded at 18.8 T that emphasize the differences between the decay rates of $C^\alpha_T H^{|\alpha\rangle}$and $C^\alpha_T H^{|\beta\rangle}$ (typically $1-2$ s^{-1}in the first few points). Included in the figures are solid lines corresponding to fits of all dispersion curves recorded from 17 residues that satisfy the criteria listed in the Materials and Methods.

Values of $D^B_{C\alpha,H\alpha}$ were calculated from measured $\Delta D_{C\alpha,H\alpha}$ and $D^A_{C\alpha,H\alpha}$. Figure 6 shows the correlation plot between dipolar coupling values ($D^B_{C\alpha,H\alpha}$) of the invisible state, *PL* (7% *L*), measured using the spin-state selective CPMG approach (*y* axis) vs. the corresponding couplings measured directly from a fully bound sample. Data points indicated with circles are those for which the signs of $\Delta D_{C\alpha,H\alpha}$ ($\Delta\nu$) were obtained as described above using the method of Skrynnikov et al.[43] Squares denote data points for which the sign of $\Delta\nu$ (and hence the value of $D^B_{C\alpha,H\alpha}$) was obtained from chemical shifts of *P* and *PL*, measured directly on samples where *P* or *PL* is the dominant species. It is clear that a very good correlation is obtained. As a final note it is important to emphasize that although we have

(55) Tjandra, N.; Omichinski, J. G.; Gronenborn, A. M.; Clore, G. M.; Bax, A. *Nat. Struct. Biol.* **1997**, *4*, 732–738.
(56) Tjandra, N.; Bax, A. *J. Magn. Reson.* **1997**, *124*, 512–515.
(57) Yang, D.; Tolman, J. R.; Goto, N. K.; Kay, L. E. *J. Biomol. NMR* **1998**, *12*, 325–332.
(58) Messerlie, B. A.; Wider, W.; Otting, G.; Weber, C.; Wuthrich, K. *J. Magn. Reson.* **1989**, *85*, 608–612.

assumed that J_{CH} values are the same in the ground and excited states in the analysis here, scalar coupling values in the excited-state can be measured independently by repeating the $^{13}C^{\alpha}$ spin-state selective measurements on an unaligned sample. This was not done presently, however.

Concluding Remarks

We have presented experiments for measuring $D_{CO,HN}$ and $D_{C\alpha,H\alpha}$ residual dipolar coupling values in invisible states and verified that accurate couplings can be obtained in a simple exchanging system involving ligand binding to a protein. These experiments complement previously published methods for quantifying $D_{N,H}$ and for measuring changes in ^{13}CO chemical shifts upon alignment.[19,24] In addition, supplementary information in the form of ^{15}N, ^{1}HN, $^{13}C^{\alpha}$, and ^{13}CO chemical shifts of the excited-state can also be measured.[31] Together, these four classes of chemical shifts and anisotropic interactions provide powerful restraints for quantifying structures of excited protein states and will facilitate studies of these conformers at a level of detail heretofore not possible.

Acknowledgment. This work was supported by a grant from the Canadian Institutes of Health Research (CIHR). D.F.H. and P.V. hold fellowships from the CIHR and the CIHR Training Grant on Protein Folding in Health and Disease. respectively.

JA801005N